COBEM 2021 26th International Congress of Mechanical Engineering
November 22-26, 2021, Virtual Congress, Brazil

COB-2021-1315
ASSESSMENT OF ADVANCED FERRITIC ALLOYS USED AS CLADDING MATERIALS IN NUCLEAR POWER REACTORS

Daniel de Souza Gomes
Nuclear and Energy Research Institute (IPEN/CNEN - SP), Av. Prof. Lineu Prestes 2242, 05508-000, São Paulo, SP, Brasil
dsgomes@ipen.br

Claudia Giovedi
Analysis, Evaluation, and Risk Management Laboratory (POLI / USP – SP), Av. Prof. Mello Moraes 2231, 05508-000, São Paulo, SP, Brasil.
claudia.giovedi@labrisco.usp.br

Abstract. The fuel performance code, Fuel Analysis under Steady-state and Transients (FAST), permits cladding options, such as zirconium alloys and iron-chromium-aluminum (FeCrAl). FAST code support as cladding Kanthal, CM35, and CM36 alloys. We implemented a comparative analysis between ferritic alloys, steel, and zircaloy. Many features of ferritic alloys classify as more tolerant materials, such as high resistance to steam oxidation, reduced hydrogen release, and longer coping time. But the neutron penalty must reduce cladding thickness to let a greater fuel volume. Both ferritic alloys and austenitic steel show higher corrosion resistance, also avoiding hydrogen releases. FeCrAl provides more resistant corrosion cracking than stainless steel. The properties of steel 348 are comparable to those of FeCrAl alloys. Steel exhibits superior thermal conductivity, linear thermal expansion, and mechanical strength. Both offer similar specific heat, melting points, and densities. The chemical composition of the steel has 66% iron and 19% chromium, compared with Kanthal APMT™, which uses 68.8% iron and 22% chromium. The results found real advantages related to safety risks using ferritic cladding materials.

Keywords: *Stainless Steel, Kanthal APMT, Accident Tolerant Fuel, FRAPCON, FRAPTRAN, FAST*

1. INTRODUCTION

A long-term consequence of nuclear accidents at Three-Mile Island (1979) and Fukushima (2011) was the accident-tolerant fuel (ATF) plan (Terrani, 2018). Both events resulted from the high-temperature oxidation of zirconium in contact with water steam. Zirconium oxidation is an exothermic reaction that produces hydrogen gas, increasing the risk of a hydrogen explosion and leakage of radioactive isotopes (Kim et al., 2015). There is a safety risk attached to any reactors that operate with zirconium alloy (Zircaloy) cladding. During a loss of coolant accident (LOCA), the cladding can undergo rapid oxidization following the partial melting of the core (Zinkle et al., 2014). Thus, the United States Department of Energy (DOE) introduced safety programs, such as the Advanced Fuels Campaign (AFC) under the fuel cycle research and development (FCRD) program.

The DOE maintains research plans focused on more tolerant fuel options, developing computational simulations for advanced materials (Martineau et al., 2020). The ATF coupled with AFC and FCRD achieve better nuclear security and greenhouse-gas emission-reduction objectives. Today, several efforts cover a complete range of materials, such as uranium nitride (UN), uranium silicide (U_3Si_2), Cr_2O_3-doped fuel, and SiC-UO_2 composite fuel. Thus, DOE programs develop a vast range of advanced claddings materials that can substitute zircaloys in the short term.

These plans enhance safety margins under transients, such as LOCAs and reactivity-initiated accidents (RIAs) (Gamble et al., 2017). With the increase of the refueling period over 18 months, they are attaining a huge exposition to irradiation and corrosion of materials. Changes in the regulatory limits must appear in the future, concerned with optimized discharge burnup and cycle length for pressurized water reactors (PWRs). Longer burning cycles need a high enrichment exceeding 5%. ATF plans predict a set of effects for extended burning periods, with unwanted effects of gap closure and solid contact from the pellet cladding mechanical interaction (PCMI). Several cladding options need considerations, particularly the cracking rate of zircaloy (Steinbrück and Böttcher, 2011). In addition, fuel swelling, corrosion, hydrides release must affect zircaloys under irradiation.

Today, there are 440 power reactors in service operating with fuel systems based on UO_2 and zircaloys. The next-generation reactors will see supercritical reactors with a fast neutron spectrum operating at temperatures between 620 and 650 °C, with pressures of up to 25 MPa. Next to nuclear units will soon have an average power density of 30% higher than the current units in service. Soon, nuclear units will need advanced materials with improved irradiation resistance and high creep strength (Pioro and Duffey, 2015).

The most frequent heat treatments applied for zircaloys are stress-relief annealing (SRA) and recrystallization-annealing (RXA), which offer differing susceptibility levels to hydrogen penetration into the alloy. A hydrogen absorption of over 300 ppm causes hydride embrittlement, altering the fracture toughness of zircaloy. In comparison, it affects SRA zircaloy-4 to a higher level than RXA zircaloy-4. Zircaloy systems are including iron (Fe), chromium. (Cr), and nickel (Ni) has been used to increase corrosion resistance. PWRs have employed zircaloy-4. zircaloy-2, which permits a higher Ni content, avoids nodular corrosion that generates cladding exfoliation. Since 2008, it has refueled power units with optimized ZIRLO™ or M5™ containing niobium. These alloys have a superior creep response and burnup of up to 74 MWd/KgU.

Series 300 stainless steel (SS) exhibits good long-term mechanical strength at elevated temperatures. Many steel grades contain elements with significant neutron absorption, such as nickel and chromium. For example, the composition of SS-348 contains 19% chromium and 11% nickel, and the ferritic alloy, Kanthal, has 22% chromium (Giovedi et al., 2019). From 1960 until the mid-1970s, American fleet reactors used steel as cladding before zircaloys (Abe et al., 2014). La Crosse Boiling Water Reactor (BWR) used SS-304L, then substituted by SS-348 or SS-347 with contained tantalum (Ta) and Nb as stabilizers (Giovedi et al., 2014). During the 1970 decade, it used SS cladding on four PWRs: Haddam Neck, Indian Point 1, San Onofre 1, Yankee Rowe (Giovedi et al., 2018). In Lacrosse, a BWR showed a power density of 41.4 kW/L with a fuel enrichment of 3.63%, using steel 348H as cladding, had an outer diameter of 8.89 cladding thickness of 0.508 mm. In contrast, BWRs used SS-304 showed stress corrosion cracking, exposing the vulnerability attributed to joints under sustained tensile stress (Gomes et al., 2016). The Vallecitos BWR operated with SS-304L cladding replaced by zircaloy. Big Rock Point employed SS-316. Plutonium mixed oxide fuel used nickel alloys as cladding. In BWRs, the corrosion detected around welds in contact with steam at raised temperatures.

Ferritic alloys have attracted growing interest because of their low susceptibility to intergranular and stress corrosion cracking. Today, the Oak Ridge National Laboratory (ORNL) and Global Nuclear Fuel (GNF) have produced FeCrAl alloys and seek licenses to operate commercially. Oxidation resistance FeCrAl alloys are between one and three orders of magnitude higher than Zircaloy (Gomes et al., 2017). They have an admirable mechanical response, with the yield stress being four times higher than Zircaloy (Gomes and Giovedi, 2019). FeCrAl has several formulations containing aluminum, where aluminum oxide layer (Al_2O_3) formation suppresses hot steam effects. The outer surface has a thin layer of Al_2O_3, deposited 100 times slower than ZrO_2 on zircaloys. The slow build of oxide layers results in higher corrosion resistance, more radiation resistance, reduced hydride release, and improved cladding ductility.

Over the years, technical applications produced groups of FeCrAl alloys with differing Cr content (5–15 wt.%) and Al (3-6 wt.%). The first former model, knowledge as the General Electric (GE) design, incorporated arc-melting and hot-working methods. In 2013, the ORNL released plans to focus on the strengthened oxide dispersion (ODS) route to manufacture FeCrAl alloys, a natural evolution of the GE model (Field et al., 2018). This project focuses on improving the mechanical properties to face or outpace the nuclear safety conditions (Raiman et al., 2020). ODS alloys must boost oxidation protection and radiation tolerance (Dryepondt et al., 2018). Today, ORNL has developed and assessed accident-tolerant FeCrAl alloys such as C35M (Fe-13Cr-5-Al-2Mo, wt.%), reducing ballooning burst levels and shunning the hydride effects.

1.1 Computational tools

One of the first fuel performance codes to reproduce the FeCrAl alloys was the BISON produced at Idaho National Laboratory (Hales et al., 2016). In this research, we adopted the CONstant (FRAPCON-4.0) and fuel rod analysis package TRANsient (FRAPTRAN-2.0) sponsored by the Pacific Northwest National Laboratory (PNNL). The US Nuclear Regulatory Commission (USNRC) recommended FRAPCON to license nuclear units (Geelhood et al., 2016). Both codes calculate the in-pile behavior of fuel rods in PWRs or BWRs under normal and off-normal conditions. Performance system calculates the thermal and elastic properties of fuel and cladding involved in fuel rod response. Thermal properties depend on temperature via the Arrhenius equation types. The library (MATPRO) describes physical models as fission gas release (FGR) used to predict gaseous products, like xenon and krypton, and solid contact model (FRACAS), used to assess PCMI extended to fuel deformation response. In extension, code implementing safety analyses to find out no fuel melting will arise or that the internal pressure will stand below a limit. In 2020, the Fuel Analysis under Steady-state and Transient (FAST) updated the FRAPCON-4.0 and FRAPTRAN-2.0 versions in a single combined system (Porter et al., 2020). The FAST package involves full facilities of FRAPCON-4.0 and FRAPTRAN-2.0. In extension, FAST permits analyze ATF concepts as Kanthal APMT, C26M, C35M, and HT-9 steel.

2. ANALYSIS OF CLADDING MATERIALS

For simulation analysis, it has chosen a reactivity accident using SS-348, Kanthal APMT, and ZIRLO. Reactivity accidents may occur because of a malfunction in rod ejection in PWRS or rod drop in BWRs. Under RIA scenarios, the pellet suffers a higher thermal rate carried to the fuel rod, resulting in increased thermal gradients. A short enthalpy pulse causes rapid heating and expansion, boosting the internal pressure.

Under transient conditions, strong oxidation forms hydrides released in zircaloy with the elasticity loss, which speeds up the failure process. FeCrAL alloys and steel show reduced effects from hydrides and exhibit superior mechanical strength responses. The challenge is to provide a definitive comparison of SS-348 and FeCrAl alloys with scarce empirical data.

2.1 Thermal properties

The cladding materials have various densities: SS-348 is 7.96 g/cm^3, Kanthal APMT™ is 7.25 g/cm^3, and ZIRLO™ is 6.56 g/cm^3. ZIRLO™ shows a smaller thermal neutron cross-section of 0.20 barns, and both ferritic materials exhibit a larger neutron cross-section because of their contents as nickel and iron. The neutron cross-section of SS-348 and Kanthal APMT™ is over 2.0 barns, ten times that of most zircaloys. Figure 1 presents the thermal conductivity curves of Kanthal APMT™, ZIRLO™, and SS-348 as functions of temperature.

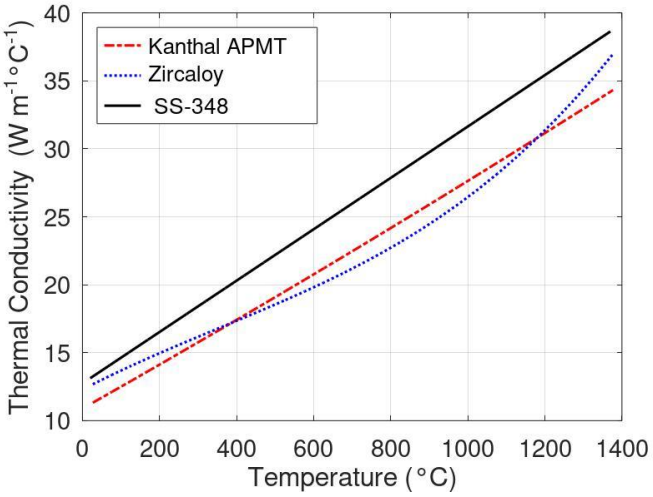

Figure 1. Thermal conductivity of Kanthal APMT, zircaloy, and SS-348

Austenitic stainless steels have a lower melting point (1398-1446 °C) but higher thermal conductivity than zircaloys. However, the Kanthal APMT™ and ZIRLO™ have a thermal conductivity average of 23 KW/m below 1450 °C. Therefore, in the temperature range of 373–1165 °C, the thermal conductivity of the Kanthal is superior to that of ZIRLO™. Zircaloy is an anisotropic material that explains different instantaneous thermal expansion coefficients across each axis. Subcode CTHEXP returns the cladding thermal expansion as a function of temperature, and ZIRLO™ shows an inflection point near the phase transition 700-850 °C. But ferritic alloys and steel do not exhibit a transition phase. Figure 2 compares the thermal expansion of Kanthal APMT™, SS-348, and the axial and diametral of ZIRLO™. Compared with steel, the ZIRLO™ has a lower thermal coefficient than Kanthal APMT™ and SS-348.

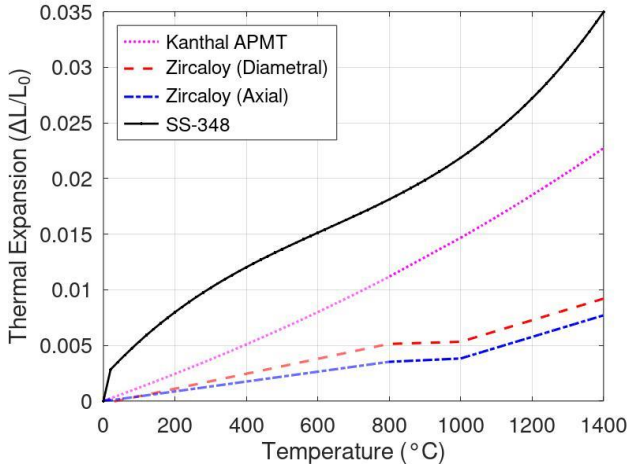

Figure 2. The thermal expansion of Kanthal APMT, SS-348, and the axial and diametral of zircaloy.

Safety analysis has as requisite to predict the thermal strain in the circumferential and axial orientation. Gap closure speeds up and arisen stress following cladding deformation leading to the onset of clad crack propagation and fuel collapse (Shinozaki et al., 2016). Kanthal APMT™ and SS-348 are isotropic materials with the same thermal expansion coefficient on any axis. A significant repercussion comes from the low conductivity of zircaloys without accounting for the irradiation effects. Zircaloy show anisotropic behavior zircaloy shows thermal expansion coefficient 6×10^{-6}/°C and 9×10^{-6}/°C on axial and circumferential, while Kanthal APMT™ is 12×10^{-6}/°C and SS-348 is 17.3×10^{-6}/°C at 25 °C. In extension, the subcode ZOEMIS calculates the surface emissivity of cladding with slight variation for each material in the analysis. The heat capacity of SS-348 increases with temperature in the solid phase below 1360 °C, varying between 464 and 690 J/kg°C. ZIRLO™ shows a structural transition from alfa to beta phases between 807 and 997 °C. The heat capacity of ZIRLO™ offers a peak point of 816 J/kg °C at 900 °C. A higher heat capacity should improve fuel safety by introducing a slower transient response. Figure 3 displays the specific heat capacities of the elements analyzed.

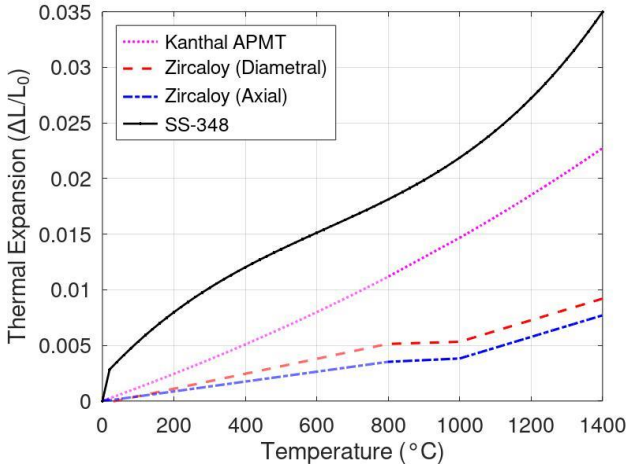

Figure 3. Heat capacity of cladding materials: Kanthal APMT, SS-348, and zircaloy

Crystal microstructure shows dependency on thermal conductivity related to grain size. CTHCON subcode calculates thermal conductivity expressed as a temperature function, for instance, Zr-4, Zr-2, ZIRLO™, optimized ZIRLO™, and M5™. Each cladding material creates distinct oxide; steel creates iron dioxide (FeO_2) and ferric oxide (Fe_2O_3), zircaloy produces zirconia (ZrO_2), and FeCrAl alloys form chromium oxides (Cr_2O_3) and aluminum oxide (Al_2O_3). Zirconia has a lower thermal conductivity than chromium oxide, and iron oxides subcode ZOTCON calculates the cladding oxide thermal conductivity. Zircaloy produces an allotropic phase transformation ($\alpha \rightarrow \beta$) between 800°C and 1000°C. Under phase change from a hexagonal closed packed structure, below 800°C, to a body-centered cubic around 1000°C. In accident scenarios, high heat rates at least 100°C/s delay phase transformation.

2.2 Mechanical properties

Mechanical properties show dependencies on temperature, composition, and microstructure. The CELMOD and CSHEAR contain correlation to describe the elastic and shear modulus as temperature-dependent, updated for Kanthal and SS-348. In contrast, irradiation growth calculates the increased axial length and cladding diameter contraction under irradiation, defined as a neutron flux function.

Martensitic steel and stainless steel had adopted the same model for irradiation growth used for zircaloy defined in CAGROW. Nuclear environments could cause severe damage to nuclear materials, inducing crystal defects, splitting on irradiation-hardening, and embrittlement. Hardening increases yield strength (YS), while embrittlement produces a decrease in elongation coupled with a reduction of fracture toughness.

Compared with Kanthal, the zircaloy has a lower elastic modulus of 99.3 GPa at 25 °C and a poison ratio of 0.33 at room temperature, increasing to 0.40 at 863 °C. In contrast, zircaloy showed a YS of 241 MPa, a UTS of 413 MPa with an elongation break of 20%. FeCrAl alloys have different tensile properties depending on thermal treatment, such as cold working, composition, also show dependency on chromium content.

FeCrAl alloys offer more tolerant cladding because of their advanced mechanical response. Indeed, FeCrAl alloys with a molybdenum (Mo) content of 3 wt.% have a high elastic modulus. Kanthal APMT™ shows linear elastic modulus as a temperature curve, reaching 220 GPa at 20 °C and reducing to 130 GPa at 1000 °C. Figure 4 displays the relationship between the elastic modulus and temperature for the three groups of alloys in the analysis. The limits of mechanical properties have a strong dependence on the melting point, and zircaloy has a higher melting point of 1850 °C.

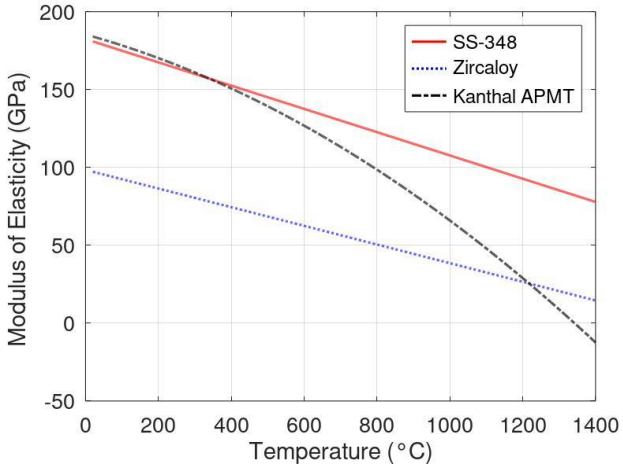

Figure 4. Elastic moduli of SS-348, zircaloy, and Kanthal APMT

In contrast, the Poisson ratio shows a slight linear increase with temperature, from 0.27 at 20 °C to 0.30 at 800 °C. The tensile properties for Kanthal APMT stay constant between 400 °C and 500 °C with a YS of 540 MPa and UTS of 740 MPa. Figure 5 shows the relationship between ultimate tensile strength and temperature for SS-348, ZIRLO™, and Kanthal APMT.

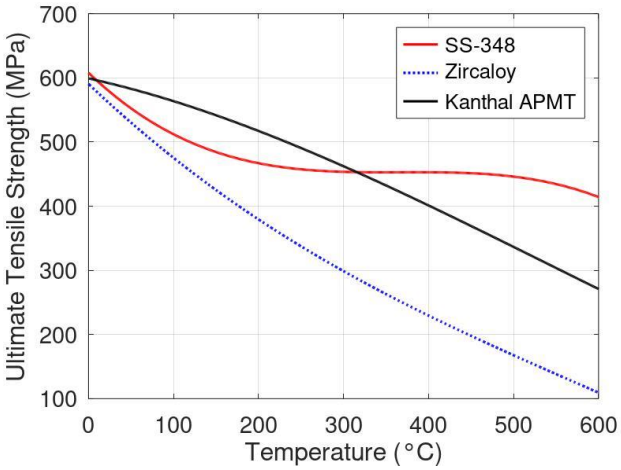

Figure 5. Ultimate tensile strength of SS-348, zircaloy, and Kanthal APMT

While ZIRLO™ has a UTS of 413 MPa and a YS of 241 MPa, Kanthal APMT™ can have a UTS of up to 740 MPa and YS of up to 540 MPa. In addition, the elongation break limit of ferritic alloys is excellent compared to ZIRLO™. The elongation break of SS-348 is 45%, for Kanthal APMT™, it is 26%, and for ZIRLO™, it is 20%.

The crystal structure of austenitic steel is austenite, defined as a solid solution of iron and carbon. Austenite does not exist below 723 °C and has a carbon concentration of 0.83%. One feature that defines austenitic steel is a minimum chromium content of 10.5% and other contents as iron and nickel. SS-348 has a higher elastic modulus reaches 195 GPa at 20 °C and reduces to zero at 1450 °C. In comparison, the Poisson ratio of SS-348 shows a linear increase with temperature, from 0.29 at 20 °C to 0.33 at 600 °C. SS-348 showed a yield strength of 275 MPa, ultimate tensile strength (UTS) of 655 MPa, and an elongation break of 45%.

3. REVIEW OF ACCIDENT SCENARIOS

There are two typical scenarios for RIA accidents: control rod ejection in PWRs and control rod drop in BWRS. An uncontrolled movement of the control rods creates a fast insertion of positive reactivity, producing a super-prompt critical state. Fuel rods suffer damage after a quick pulse of high reactivity, with 100 ms or slighter, such as cladding ballooning and bursting, embrittlement, oxidation, and limited fuel melting. First, USNRC endorsed a peak of radial enthalpy of 230 cal/g to avoid destructive forces.

The allowable limit is a function of the differences between the internal and external pressures of the rod, referenced by insertion of 65 to 170 cal/g. The RIA criteria show minor deviation for each regulatory agency because of the experimental conditions applied in each analysis performed. Thus, the failure criteria depend on the burnup level, fission gas release, hydride release, oxidation, and enthalpy inserted during the pulse. Today, regulatory agencies still adopt experimental rules. It still limited fuel cladding failure based on enthalpy insertion to 230 cal/g. Cladding failure by ballooning and bursting due to fuel enthalpy is 170 cal/g at high burnup. There is a limit of 150 cal/g for pellet-cladding mechanical interaction. Failure by oxidation-induced embrittlement had used 150 cal/g as a limit. Aqueous corrosion of zircaloy produces hydrogen or deuterium, which diffuses into diffused cladding beyond the terminal solid solubility precipitates out as brittle hydride phases. FeCrAl alloys are not susceptible to hydrogen ingress, and it affects SS to a lesser extent than zircaloy. Failure depends on earlier irradiation damage, including the linear power rate, burnup extension, and in-service cladding corrosion.

3.1 Simulation of nucelar fuel behavior

The AP1000 is a PWR 17 × 17 planned to 157 fuel assemblies, 264 fuel pins, 24 control rod guide tubes, and a neutron monitor guide pipe (Cummins et al., 2003). The fuel assembly showed three zones with enrichment of 2.35%, 3.40%, and 4.45%. AP1000 design presents a two-loop PWR generating 1117 MWe, reducing the number of items to promote simplification, security, and reliability (Schulz, 2006). Korea established an advanced power reactor (APR) with two coolant loops and reduces the temperature, to soothe the stress corrosion cracking in steam tubes. Raise the CAP-1400 design-build through collaboration between China and Westinghouse. Table 1 explains the reactor core design specifications of the AP1000 used in the simulation performed with the fuel systems.

Table 1. Thermal hydraulic core design specifications of the PWR AP1000

PWR AP1000 Nominal Design	Value
Reactor core heat output, MW(th)	3400
Average core power density, MW/m^3	109.7
Fuel assembly design	17 x 17
Nominal system pressure, MPa	15.51
Primary coolant flow rate, kg/s	14300
Inlet coolant temperature, °C	279.4
Active fuel length, m	4.267

For each cladding material, it found damaged scales produced by irradiation, degrading the strength properties. Zircaloy absorbs hydrogen, reducing the zircaloy performance, but does not detect Kanthal and SS-348. During the burn cycle, PWRs exhibit neutron irradiation doses of up to 100 displacements per atom (dpa) on the fuel rod by the end of the irradiation cycle. Table 2 shows the spatial changes to compensate for the observed material limits.

Table 2. AP1000 PWR 17 × 17 fuel rod dimensions

Fuel Properties	Zr-4	SS-348	FeCrAl
Fuel outer diameter, mm	9.5	9.5	9.5
Cladding thickness, mm	0.57	0.51	0.35
Gap thickness, mm	0.082	0.082	0.082
Pellet outer diameter, mm	8.1915	8.3185	8.6335
Pellet length, mm	9.387	9.387	9.387
Enrichment U^{235}, %	4.45	4.59	4.59

One most common failure mode during RIA results from pellet cladding mechanical interaction because of the rapid thermal expansion of the fuel pellet. Simulation analysis had advised to decrease the cladding thickness and increase the diameter of the fuel pellet when using FeCrAl alloys and stainless steel to compensate thermal cross-section. Under regular services, the enhanced conductivity of Kanthal APMT™ and SS-348 shows a slight reduction in centerline temperature compared with ZIRLO™ at 2 °C for SS-348 and 16 °C for Kanthal APMT™. However, under a short enthalpy pulse, the fuel rod will fail. But cladding thickness of Kanthal APMT shows a thickness of 0.419 mm. Kanthal supports a higher enthalpy peak than zircaloy, although cladding thickness reduced to zircaloy of 0.572 mm. The regulatory guide DG-1327 still uses an empirical database to define safety limits. This guide defined fuel cladding failure thresholds for ductile failure, brittle failure, and PCMI, only for zirconium alloys (Brown et al., 2020). Figure 6 displays the fuel centerline temperature for 1600 effective power days for the cladding materials in the analysis. In extension, the total FGR would include the steady-state fission product gap inventory, plus any gas released during RIA transient.

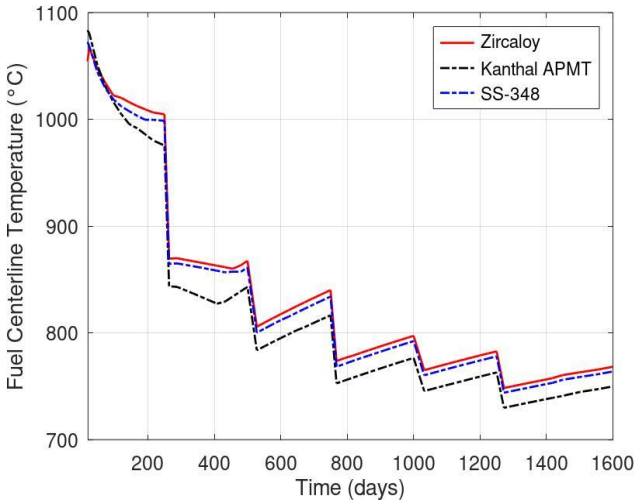

Figure 6. Fuel centerline temperature between zircaloy, SS-348, and Kanthal APMT

In the simulation, the irradiation cycle shows 1600 effective power days divided into five groups using a linear power rate of 24, 20, 18, 15, and 14 kW/m following the AP1000 specifications, achieving over 55 MWd/KgU. The FRAPCON has four fission gas release models, and the most used is the ANS-5.4 model developed by the American Nuclear Society and updated in 2011. Besides, the fission gas comprises xenon and krypton, which degrade the thermal conductivity and increase the internal pressure of the fuel rod, which affects the mechanical responses. The corrosion kinetics model defines time and temperature functions, with a weak dependence on burn cycle extension. Figure 7 shows the fission gas release for ZIRLO™, Kanthal APMT™, and SS-348 grade.

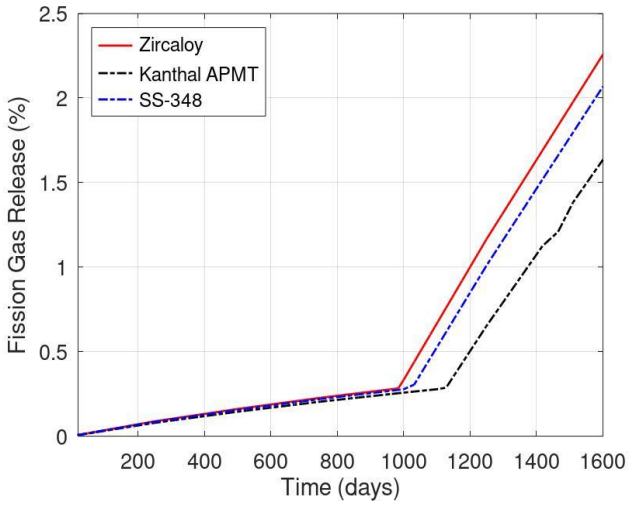

Figure 7. Fission gas release production for zircaloy, SS-348, and Kanthal APMT

The burn cycle used five batches in the simulation using a linear power rate of 24, 20, 18, 15, and 14 kW/m following the AP1000 specifications. The pulse of enthalpy used forms a Gaussian curve with a total width of 11.8 ms. If it uses a triangular shape, the base is 30 ms. Fission products increase the pressure and decrease the thermal conductivity. In addition, the production and release of fission gases depend on several factors, such as extending the irradiation cycle and power history. The ZIRLO™ showed failure at the insertion of 10000 KW/s for a pulse width equivalent to 170 cal/g.

The fuel centerline temperature and FGR calculated for ZIRLO™ were higher than Kanthal APMT™ and SS-348 during regular operation. The FRAPCON supports the quantitative FGR model, ANS-5.4, developed by the American Nuclear Society and updated in 2011 Table 3 shows the parameters for the fuel simulation under regular operation. The swelling model depends on the temperature, burnup levels, and porosity. As mentioned, FeCrAL alloys and SS-348 produce different oxides than zircaloy, but the corrosion model depends on the time and temperature and weakly on the burnup level.

Table 3. Results from steady-state simulation using the cladding materials in analysis

Fuel Peak Response	ZIRLO™	Kanthal APMT™	SS-348
Fission Gas Release, %	2.25	1.65	2.06
Fuel Centerline Temperature, °C	1108	1106	1097
Cladding Strain Increment, %	0.025518	0.02476	0.025054
Gap Gas Pressure, MPa	11.06	9.56	10.89

3.2 Failure threshold under accident conditions

During the active life of the PWR, it controlled nuclear fission within the reactor core using control rods. AP1000 uses 69 control rods, divided into black rods applying an absorber (Ag-In-Cd) and gray rods using a combination of neutron poison and tungsten rods. The RIA is a design-basis accident studied for PWR. Figure 8 shows the fuel centerline temperature after a short enthalpy pulse with insertion of 175 cal/g, where the fuel rod does not cause failure.

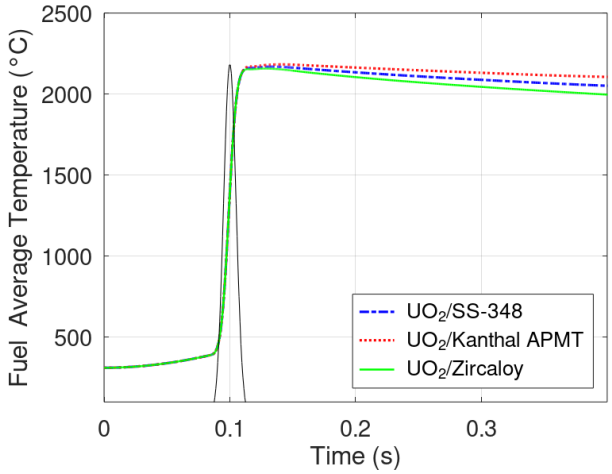

Figure 8. The temperature of UO_2 fuel with zircaloy and SS-348, after short enthalpy pulse insertion of 175 cal/g

Under RIA accident had two consecutive phases: the first phase comprises the PCMI phase, followed by the departure from the nucleate boiling (DNB) phase. Gap closure is present in the middle of the burn cycle, followed by a brief pulse of enthalpy for each case. The DNB phase starts at the boiling point of the coolant, which leads to a substantial reduction in the thermal transfer between the fuel rod and water. Insertion induces a heat-up rate to exceed 1000 °C/s, causing temperatures to exceed 900 °C. Zircaloys exhibit an allotropic phase transformation ($\alpha \rightarrow \beta$), and the mechanical response is unstable during the phase change. The crystal lattice structure of zircaloys changes from hexagonal close-packed (HCP) to body-centered cubic (BCC) between 700 °C and 850 °C. During the two phases, the creep behavior increases around five times the Norton exponent of the power creep law needed for the secondary creep model used at elevated temperatures up to 850 °C.

In addition, the hydrogen content precipitated in cladding over 300 ppm decreased by four times the secondary creep rate. FRAPTRAN and FRAPCON fuel codes used the classical mechanical model FRACAS-I. However, this is a rigid model that does not account for the stress-induced deformation of the fuel. It includes pellet thermal expansion, rod internal gas pressure, plastic response, and the secondary creep model. When the cladding strain passed the instability limit, it lost its cylindrical shape, and ballooning deformation occurred. BALON2 is a ballooning model that predicts strain failure, given as a function of temperature.

The fuel failure threshold is a necessary condition, as determined by the computational package FRAPTRAN. Most of the experiments performed to measure RIA behavior used stagnant water, fresh fuel, and short burnup. Exist dependence of the rod failure limit with cladding thermal behavior until quenching and the cooling conditions. The computational simulation code recovers the last conditions from FRAPCON and uses the same cooling condition with temperatures of 310 °C and a pressure of 15.51 MPa. Here, Kanthal APMT™ and SS-348 under oxidation did not make an enormous amount of hydrogen. However, SS-348 is more susceptible to stress corrosion cracking than Kanthal APMT™. In addition, the thermal expansion of ZIRLO™ was less than that of SS-348 and Kanthal APMT. Figure 9 shows the effective elastic-plastic strain curve after the enthalpy pulse insertion. The primary trouble is the significant possibility of stainless steel, and Kanthal APMT will suffer a partial melting point at temperatures up to 2000 °C.

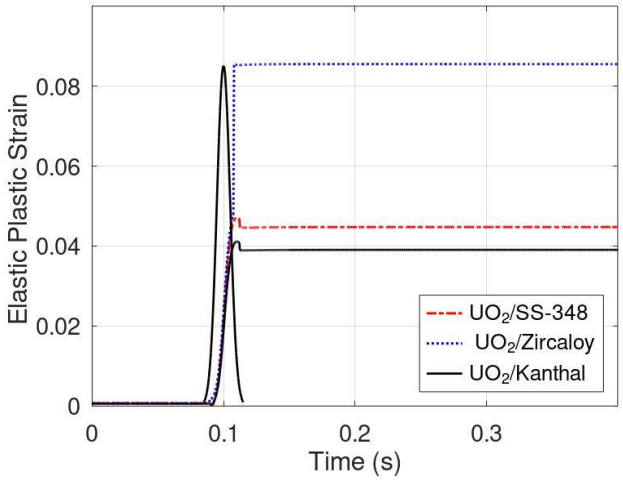

Figure 9. Effective elastic-plastic strain curve of UO_2 with SS-348 and zircaloy

4. CONCLUSION

The primary aim of the ATF plan is to avoid the expulsion of radioisotopes in the environment. The oxidation of zircaloys at elevated temperatures produces hydrogen with an explosion risk. As a result, it improved the enhanced ultimate tensile strength and creep rates for SS-348 and Kanthal APMT™ during accident scenarios. The PCMI limit is not the only relevant cladding performance limit during RIA, but the failure occurs with an elevated temperature phase caused by a boiling crisis. The simulation results showed slight differences in the fuel response. During the regular operation, the fuel behavior results are compatible with the thermal physical properties. Thus, a good forecast level under regular services, such as reduced fuel centerline temperature, decreased fission gas release, and reduced cladding strain because of the enhanced mechanical response of FeCrAl alloys, is essential. Under transient conditions, Kanthal APMT™ can exhibit a desirable performance, whereas SS-348 is like zircaloy. However, the failure limit found is slightly superior to zircaloy compared with steel and zircaloy, because of the reduced thickness planed. In extension, Kanthal and SS-348 avoid hydrogen release and explosion risk.

5. ACKNOWLEDGEMENTS

The authors are grateful to the Nuclear Energy Research Institute (IPEN) and the National Nuclear Energy Commission (CNEN).

6. REFERENCES

Abe, A., Giovedi, C., Gomes, D.S. and e Silva, A.T., 2014. “Revisiting stainless steel as PWR fuel rod cladding after Fukushima Daiichi accident.” *Journal of Energy and Power Engineering*, Vol. 8(6).

Brown, N.R., Garrison, B.E., Lowden, R.R., Cinbiz, M.N. and Linton, K.D., 2020. “Mechanical failure of fresh nuclear grade iron–chromium–aluminum (FeCrAl) cladding under simulated hot zero power reactivity-initiated accident conditions.” *Journal of Nuclear Materials*, Vol. 539, p.152352.

Cummins, W.E., Corletti, M.M. and Schulz, T.L., 2003, “Westinghouse AP1000 advanced passive plant.” In Proceedings of *ICAPP* (Vol. 3, pp. 4-7).

Dryepondt, S., Unocic, K.A., Hoelzer, D.T., Massey, C.P. and Pint, B.A., 2018. “Development of low-Cr ODS FeCrAl alloys for accident-tolerant fuel cladding.” *Journal of Nuclear Materials*, Vol. 501, pp. 59.

Field, K.G., Snead, M.A., Yamamoto, Y. and Terrani, K.A., 2018. “Handbook on the material properties of FeCrAl alloys for nuclear power production applications” ORNL/TM-2017/186. Oak Ridge National Laboratory. (FY18 Version: Revision 1).

Gamble, K.A., Barani, T., Pizzocri, D., Hales, J.D., Terrani, K.A. and Pastore, G., 2017. “An investigation of FeCrAl cladding behavior under normal operating and loss of coolant conditions.” *Journal of Nuclear Materials*, Vol. 491, pp. 55.

Geelhood, K.J., Luscher, W.G., Raynaud, P.A., and Porter, I.E., 2015 FRAPCON-4.0: A Computer Code for the Calculation of Steady-State, Thermal-Mechanical Behavior of Oxide Fuel Rods for High Burnup.

Giovedi, C., Martins, M., Abe, A., Muniz, R., Gomes, D.S. and Silva, A.T., 2018. Fuel performance assessment of enhanced accident tolerant fuel using iron-based alloys as cladding In Proceedings water reactor fuel performance meeting (WRFPM) TOPFUEL.

Giovedi, C., Abe, A., Gomes, D.S., Cherubini, M. and D'Auria, F., 2014. "Comparison of fuel performance codes using stainless steel as cladding material." In Proceedings, water reactor fuel performance meeting (WRFPM) TOPFUEL.

Giovedi, C., Abe, A., Muniz, R.O.R., Gomes, D.S., Silva, A.T. and Martins, M.R., 2017. "Analysis of the combined effects on the fuel performance of UO2-BeO as fuel and iron-based alloy as cladding." In Proceedings water reactor fuel performance meeting (WRFPM) TOPFUEL.

Gomes, D.S. and Giovedi, C., 2019. "Comparative analysis of silicon carbide with zirconium-based alloys" In International Nuclear Atlantic Conference (INAC).

Gomes, D.S., Abe, A., Silva, A.T, Giovedi, C. and Martins, M.R., 2016. "Evaluation of corrosion on the fuel performance of stainless-steel cladding." *EPJ Nuclear Sciences and Technologies*, Vol. 2, p. 40.

Gomes, D.S., Muniz, R.O.R. and Giovedi, C., 2017. "Improving performance with accident tolerant-fuels" In International Nuclear Atlantic Conference (INAC).

Hales, J.D., Williamson, R.L., Novascone, S.R., Pastore, G., Spencer, B.W., Stafford, D.S., Gamble, K.A., Perez, D.M., and Liu, W., 2016 BISON Theory Manual the Equations behind Nuclear Fuel Analysis (No. INL/EXT-13-29930). Idaho National Lab. (INL), Idaho Falls, ID United States, pp. 156.

Kim, H.G., Kim, I.H., Park, J.Y. and Koo, Y.H., 2015. "Application of coating technology on zirconium-based alloy to decrease high-temperature oxidation" In Zirconium in the Nuclear Industry: 17th Vol. ASTM International.

Martineau, R., Andrs, D., Carlsen, R., Gaston, D., Hansel, J., Kong, F., Lindsay, A., Permann, C., Slaughter, A., Merzari, E., Hu, R., Novak, A. and Slaybaugh, R., 2020. "Multiphysics for nuclear energy applications using a cohesive computational framework." *Nuclear Engineering and Design*, Vol. 367, p. 110751.

Pioro, I. and Duffey, R., 2015. "Nuclear power as a basis for future electricity generation." *Journal of Nuclear Engineering and Radiation Science*, Vol. 1(1).

Porter, I.E., Geelhood, K.J., Colameco, D.V., Torres, E.E., Luscher, W.G., Kyriazidis, L. and Goodson, C.E., 2020. "FAST-1.0: A computer code for thermal-mechanical nuclear fuel analysis under steady-state and transients Prepared for the U.S" Department of Energy, PNNL 29720, pp. 224.

Raiman, S.S., Field, K.G., Rebak, R.B., Yamamoto, Y. and Terrani, K.A., 2020. "Hydrothermal corrosion of 2nd generation FeCrAl alloys for accident tolerant fuel cladding." *Journal of Nuclear Materials*, Vol. 536, p. 152221.

Schulz, T.L., 2006. "Westinghouse AP1000 advanced passive plant." *Nuclear engineering and design*, vol. 236(14-16), pp. 1547-1557.

Terrani, K.A., 2018. "Accident tolerant fuel cladding development: Promise, status, and challenges." *Journal of Nuclear Materials*, Vol. 501, pp. 13.

Zinkle, S.J., Terrani, K.A., Gehin, J.C., Ott, L.J. and Snead, L.L., 2014. "Accident tolerant fuels for LWRs: A perspective." *Journal of Nuclear Materials*, Vol. 448(1-3), pp. 374.

7. RESPONSIBILITY NOTICE

The authors are the only responsible for the printed material included in this paper.